CHAPTER 3

ION TRANSPORT MECHANISM IN GLASSES: NON-ARRHENIUS CONDUCTIVITY AND NON-UNIVERSAL FEATURES

3.1 INTRODUCTION

Alkali ion conducting glasses are attractive solid electrolyte materials since their tuneable property by varying chemical composition to large extent and hence adapted to specific needs [1, 2]. High ionic conductivities are needed for optimizing the glassy electrolytes in various applications and it is important to find methods for enhancing them in a more systematic manner. In this context, an adequate understanding of the temperature and composition dependence of ion transport necessitates microscopic information involving both network structure and dynamics. In the liquid state, as a result of progressive structural change leads to the creation of defects, this may be retained by appropriate quenching to the glassy state. These types of intrinsic structural defects are important in that they may help to explain the diffusion of mobile species in the matrix through which they move in.

Silicate and alkali modified silicate glasses are typical glass-forming system well suited for investigating the transport and dynamics of mobile species [3, 4]. A key aspect of their short-range structure is the distribution of Q^n species (n = 0-4), meaning that different kinds of SiO_4 tetrahedra present, where the superscript n corresponds to the number of the bridging oxygen (BO) atoms and 4-n is the number of non-bridging oxygen (NBO) atoms present. The Q^n speciation depends strongly on the alkali oxide content, temperature, pressure and, thermal history. In recent decades, significant progress has been made by combining both in-situ high temperature Raman and NMR techniques to quantify the Q^n species in the different silicate glasses [5-10]. The abundance of the Q^n species is shown to be controlled by how these BOs are distributed in the network structure and follows the temperature-dependent equilibrium reaction.

$$2Q^n \Longleftrightarrow Q^{n+1} + Q^{n-1} \quad (n=1\text{-}3) \qquad (1)$$

Temperature dependence of speciation is of particular importance, given the significant variations of the physical properties with the changing temperature. It has been observed in the different glasses that, with the increase of temperature, the equilibrium reaction given in eq 1 shifts towards right hand side. Therefore, local configurations around alkali ion in the network structure become strongly dependent on the type of Q^n species associated with it.

Originally, the non-Arrhenius behaviour (nAB) in the dc conductivity has been observed in several fast ion conducting (FIC) glasses as well as in crystals, which exhibit high ionic conductivity at room temperature [11-13]. Moreover, it has been assumed that the observed nAB is characteristic feature of solid electrolyte which possesses the high ionic conductivity. Based on the experimental findings, several theoretical models have been developed to explain the observed nAB in ion conducting glasses but all these models give different insights into the ion hopping mechanisms without considering the structural details [14-16]. Recently, Malki et al observed nAB in the temperature dependence of dc conductivity in binary potassium silicate glasses with high alkali oxide content level [17]. Though the potassium silicate glasses are not good ionic conductors at room temperature but it turns out to show nAB at high alkali oxide content level and at high temperatures (well below the T_g). They recovered the Arrhenius behaviour from nAB, which is facilitated by annealing processes leading to a densification of the glasses similar in fashion with FIC glasses. The authors have used both the constraint theory and point defect model to account for the observed non-Arrhenius behaviour. However, the constraint theory approach is more macroscopic and focused more on a critical composition, which does not provide complete microscopic information about the ion transport mechanism. In contrast to nAB with negative curvature, alkali modified borate glasses found to show nAB with positive curvature in the Arrhenius plot [18]. It has been shown that the observed nAB is exclusively related to changes in the relative concentration of BO_3 and BO_4 units in glass and melts depending upon the rate of quenching. Thus, a compelling experimental identification of cause for nAB has not yet been provided.

In this work, we provide new information about the influence of silicate speciation on alkali ion transport in more detail by taking ac conductivity

measurements and high temperature Raman spectroscopy on alkali/alkaline-earth modified silicate glasses. We find deviations from Arrhenius behaviour in the dc conductivity, which can be correlated to change in the type of Q^n species associated with alkali ions. More qualitatively, we show that these deviations can be directly related to the changes in the concentration of Q^n species, which leads to the creation of new vacant sites for ion hopping with increasing temperatures. In particular, it is remarkable that the observed non-Arrhenius behavior in the dc conductivity and their structural speciations are clearly distinct from what is observed commonly in ion conducting glasses, i.e., completely reversible in nature.

3.2 EXPERIMENTAL SECTION

Three different glass compositions were selected for the present study,

$0.244\ Na_2O{\cdot}0.269\ CaO{\cdot}0.026P_2O_5{\cdot}0.461SiO_2$ (45S5)

$0.201\ Na_2O{\cdot}0.222\ CaO{\cdot}0.026P_2O_5{\cdot}0.551SiO_2$ (55S4.3)

$0.177\ Na_2O{\cdot}0.196\ CaO{\cdot}0.026P_2O_5{\cdot}0.601SiO_2$ (60S3.8)

Bulk glass samples were obtained by conventional melt quenching method. To reduce the internal stresses, as-prepared glass samples were annealed 30 K below their glass transition temperatures for 5 h and then cooled to room temperature with a rate of 1K/min (we refer these glass samples are “normal glasses”). Besides, we have prepared glass samples by adopting extended annealing (for 48 h) procedures on 45S5 and 55S4.3 glass samples to test the effect of thermal history on the electrical conductivity and their local structure (we refer these glass samples are “annealed glasses”). Following annealing, the glass samples were then ground to their requisite sizes, and the surfaces were polished, and metal electrodes consisting of silver and platinum layer were sputtered onto each surface.

Conductivity measurements were carried out by using a Novocontrol α-S high resolution dielectric analyzer in a frequency range from 10 mHz to 3 MHz, and temperature ranging from room temperature to 633 K. The temperature evolution of

Raman spectra of normal and annealed glass samples were recorded in the 1800 back scattering geometry, using a 532nm excitation of a frequency doubled Nd-YAG solid state laser (model GDLM-5015 L, Photop Suwtech Inc., China) and a custom built Raman spectrometer equipped with a SPEX TRIAX 550 monochromator and a liquid nitrogen cooled CCD (Spectrum One with CCD 3000 controller, ISA Jobin Yovn - SPEX). Laser power at the sample was 8 mW, and a typical spectral acquisition time was 2 min. The spectral resolution was 2 cm^{-1}. The temperature was controlled with an accuracy of 0.1 K by using a temperature-controller (Linkam TMS 94) equipped with a heating stage unit (Linkam THMS 600). The Raman spectra were collected from room temperature to 873 K and deconvolution procedure has been adopted to get the quantitative estimation of Q^n species on the baseline corrected spectrum. In particular, the high frequency region from 800 to 1200 cm^{-1} was analysed, where the Si-O-stretching vibrations of various SiO_4 units (Q^n) are located in this region. The deconvolution of high temperature Raman spectra were carried out by taking into account the parameters at the room temperature.

3.3 RESULTS AND DISCUSSION

In Figure 3.1, we present the frequency dependent conductivity spectra of glassy 45S5 glass sample measured over wide range of temperatures. All spectra show the frequency and temperature dependences which are typical of most ionic conductors. Further, the frequency-dependent conductivity spectra are characterized by well-defined low frequency plateaux, where the conductivity is identical to the dc ionic conductivity. These plateaux allow us to determine the dc conductivity more precisely with an error of less than 2 % and are shown in Figure 3.2 for all the three glass compositions of normal glasses. First, one observes that in all the glasses at low temperatures, the measured dc conductivity follows the simple Arrhenius form, i.e.

$$\sigma_{dc}T = \sigma_o \exp(-E_a^{dc}/k_BT) \quad (2)$$

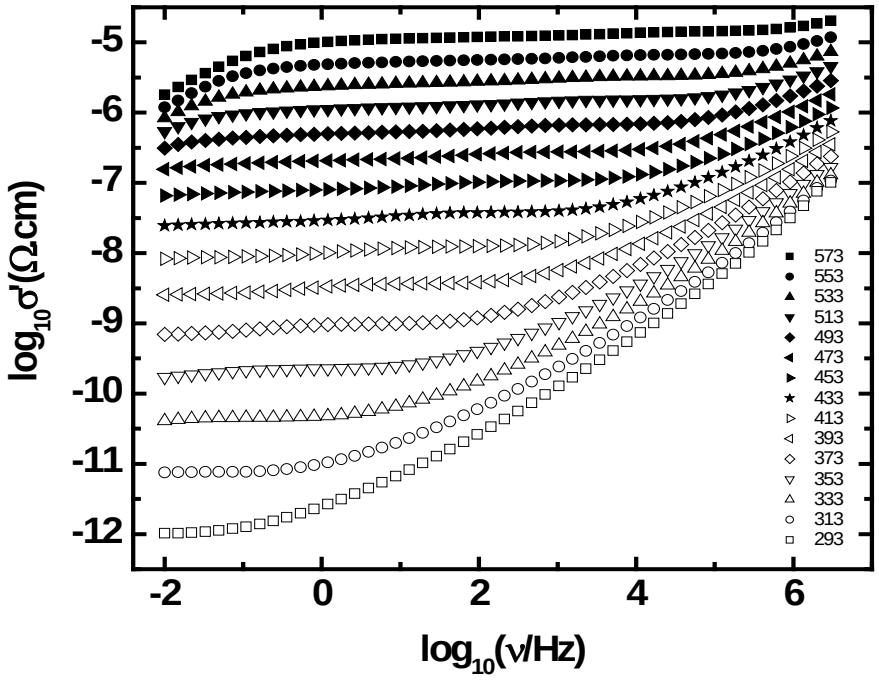

Figure3.1: *Experimental frequency dependent conductivity spectra of 45S5 glass sample at different temperatures.*

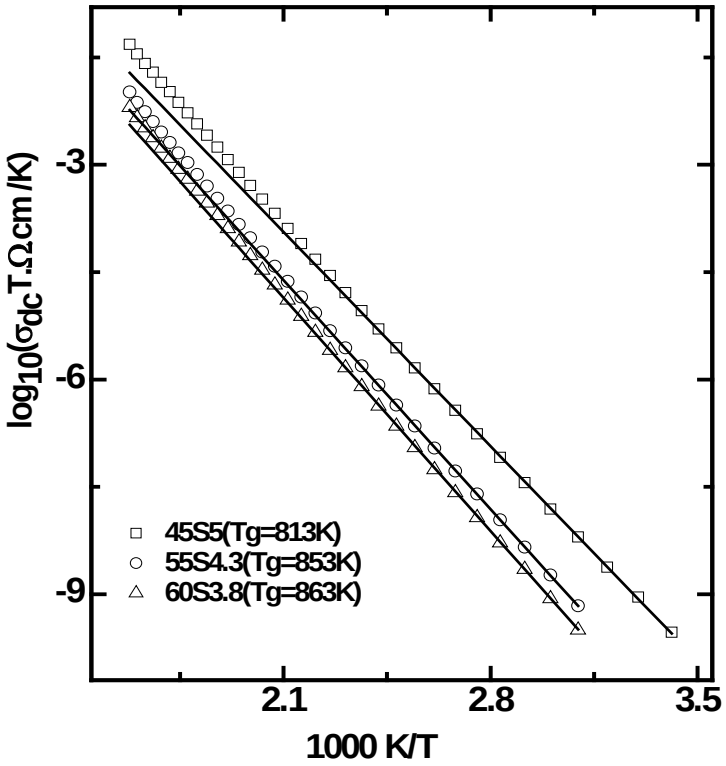

Figure 3.2: *Arrhenius plot of the dc conductivity (multiplied with temperature) of 45S5, 55S4.3 and 60S3.8 normal glasses. The symbols represent experimental data points and the fitted line corresponds to using Arrhenius law.*

Clearly, at higher temperatures, the measured dc conductivity deviates from the Arrhenius law and shows upward curvatures, i.e. a gradual increase in the slope when the temperature is increased. However, with increasing silica content (55S4.3 and 60S3.8 glasses), the onset of non-Arrhenius behavior shifts to higher temperatures, relative deviations from Arrhenius behavior becomes weak. In this context, it is worthwhile to consider the earlier ion transport investigations on 45S5 glass, where a similar nAB has been observed in the Arrhenius plot [19, 20].

Furthermore, we would like to clarify that the observed nAB is not due to the contribution from the Ca^{2+} ions at high temperatures. Since, it has been reported in the literature that activation energy for the diffusion of the alkaline-earth ions in the range from 1.5 to 2.4 eV depending on the concentration of alkali and alkaline-earth oxide content [21, 22].

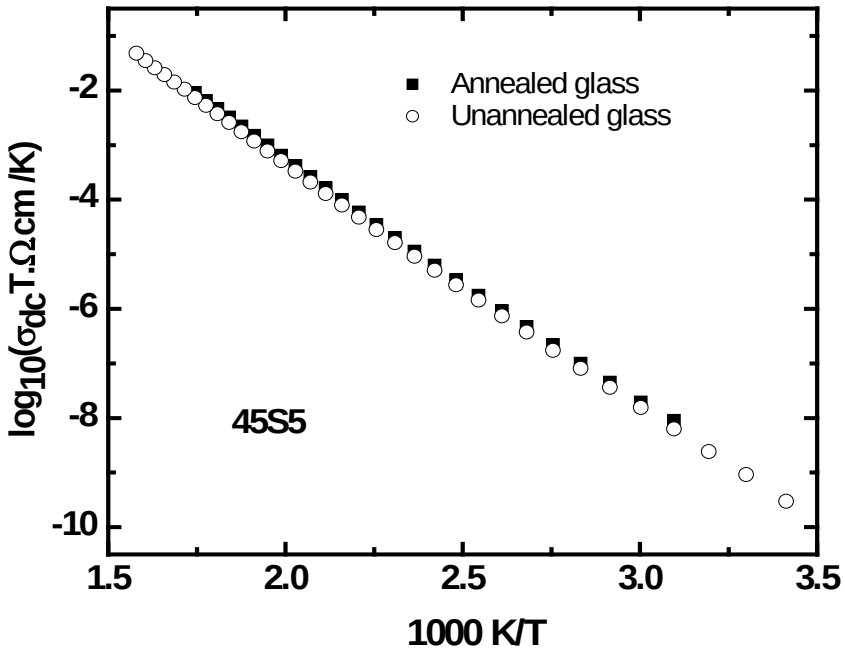

Figure 3.3: *Arrhenius plot of the dc conductivity (multiplied with temperature) of 45S5 annealed and unannealed glass.*

The temperature at which the nAB starts (e.g., 473 K for the 45S5 glass sample) corresponds to the activation energy of 0.92 eV is much smaller than those reported for the Ca^{2+} ions diffusion. Thus the observed nAB is not associated either with Ca^{2+} ions or rearrangement of the glass network due to the proximity to the glass transition

temperature and solely due to diffusion of alkali ions. Further, Figure 3.3 emphasizes the fact that even after extended annealing on 45S5 glass sample (i.e., annealed at 783 K for 48 h and T_g = 813 K), the curvature in the Arrhenius plot persists. Therefore, the recovery of Arrhenius behaviour is not enhanced with the extended annealing of glass samples, which is in contrast to the earlier observations in FIC glasses, potassium silicate, and alkali-borate glasses [11-13, 17, 18].

Additionally, we have analysed the frequency dependent conductivity spectra of all these glasses by using the Summerfield scaling law. In Figure 3.4, we show the representative scaled isotherm of the real part of the conductivity, $\sigma'(\nu)$ of 45S5 glass sample, and it clearly shows that all isotherms collapse to single master curve, obeying time temperature superposition principle (TTSP) by using the summerfield scaling law. Therefore, it seems likely that structural peculiarities of these glasses are responsible for the observed non-Arrhenius behaviour in the dc conductivity.

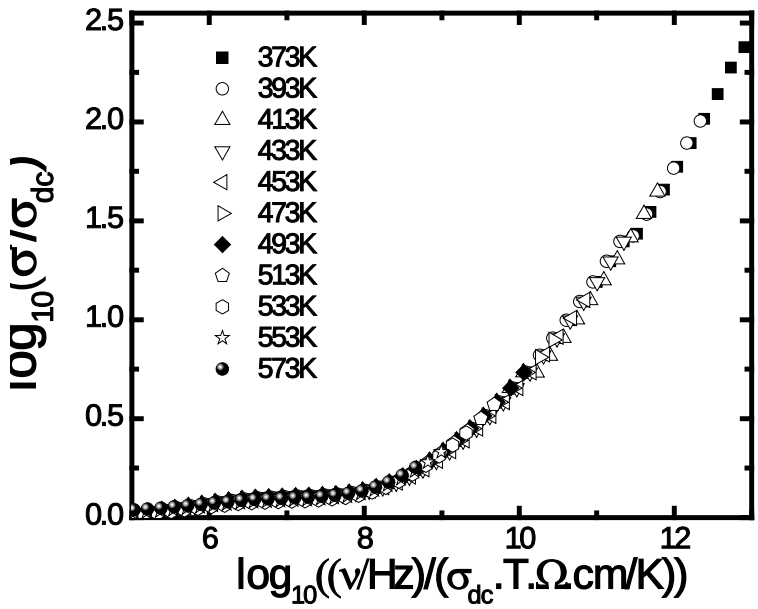

Figure 3.4: *Scaled Isotherms of the real part of the conductivity, σ'(ν), of the 45S5 glass.*

In order to understand the influence of local atomic structure on the ion transport mechanism, we have used high-temperature Raman spectroscopy as tool to reveal the nature of anionic species where the alkali ions are associated. In Figure 3.5, we represent the room temperature Raman spectra of normal glasses in the present

investigation. There is a broad, asymmetric peak at 550 to 650 cm^{-1}, which is due to the characteristic bending vibrations of silicate network and the peak maxima shifts to higher wavenumber with increasing alkali oxide content [23].

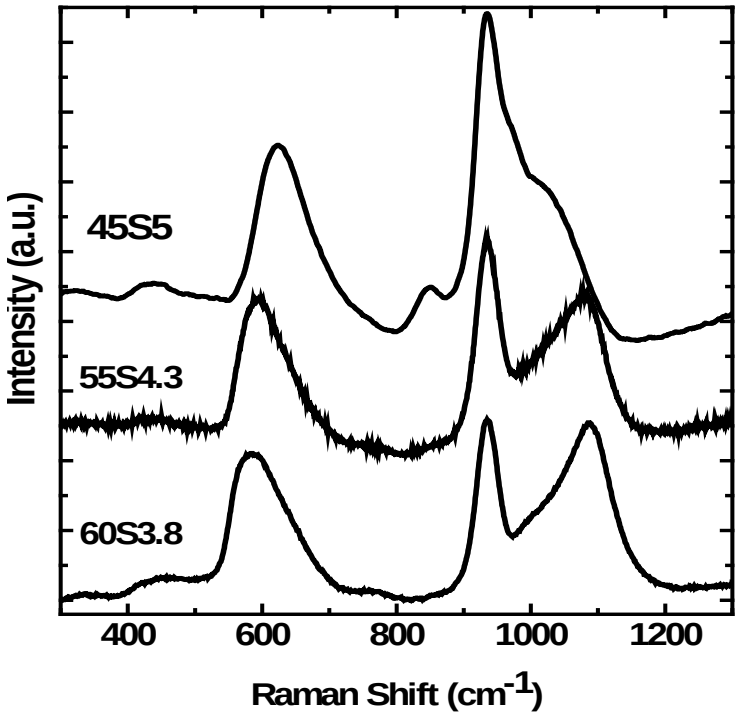

Figure 3.5: *Room temperature Raman spectra of 45S5, 55S4.3 and 60S3.8 glasses.*

Figure 3.6 and 3.7 represents high temperature Raman spectra for 45S5 and 55S4.3 glass compositions. Here, we are interested mainly in the spectral range between 850 and 1200 cm^{-1}, where the stretching vibrations of the different Q^n species are present. Thus, the high frequency region of Raman spectra was deconvoluted into four or five Gaussian bands in order to evolutes the relative abundance of different Q^n species on temperatures. Before analysing the temperature dependent Q^n species variation, we schematically represent the various types of Q^n species present in silicate and phosphate glasses are shown in Figure 3.8.

Apparently, the spectra for the 60S3.8 and 55S4.3 glass compositions are nearly similar, where the well resolved peak maxima at 945 and 1080 cm^{-1} are assigned to Q^2 and Q^3 silicate species. Although the phosphate content is small in the studied glasses, but the structural evolution of their anionic species cannot be neglected and it plays major

role on species exchange with silicate Q^n units [24, 25]. In the studied glass compositions, phosphate anionic species are found to be ortho- $(PO_4^{3-})Q_P^0$ and pyrophosphate $(P_2O_7^{4-})$ Q_P^1 units [25-27].The frequency assignment of distinct groups of silicate and phosphate species based on comparisons of the Raman spectra of isochemical crystals as well as theoretical calculations of the Raman spectra and NMR results [24-28].

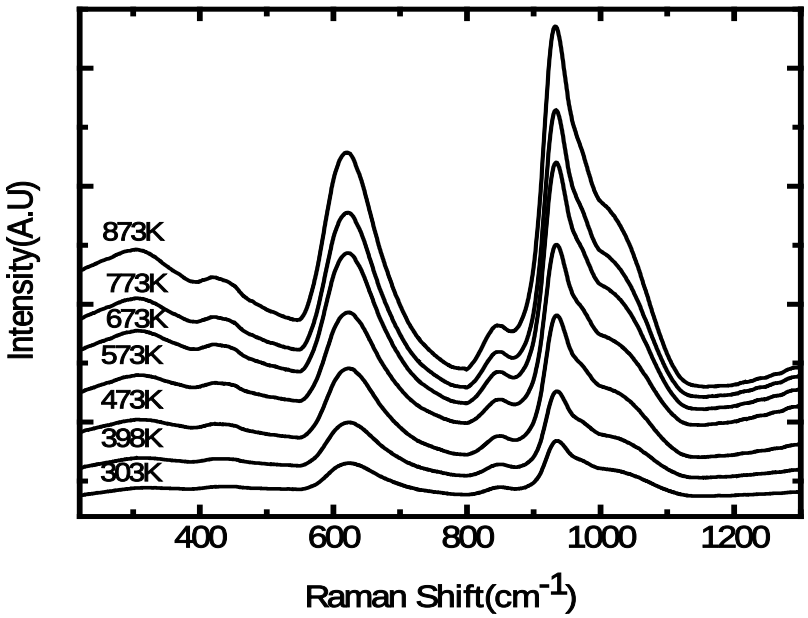

Figure 3.6: *Temperature-dependent Raman Spectra for 45S5 normal glass sample.*

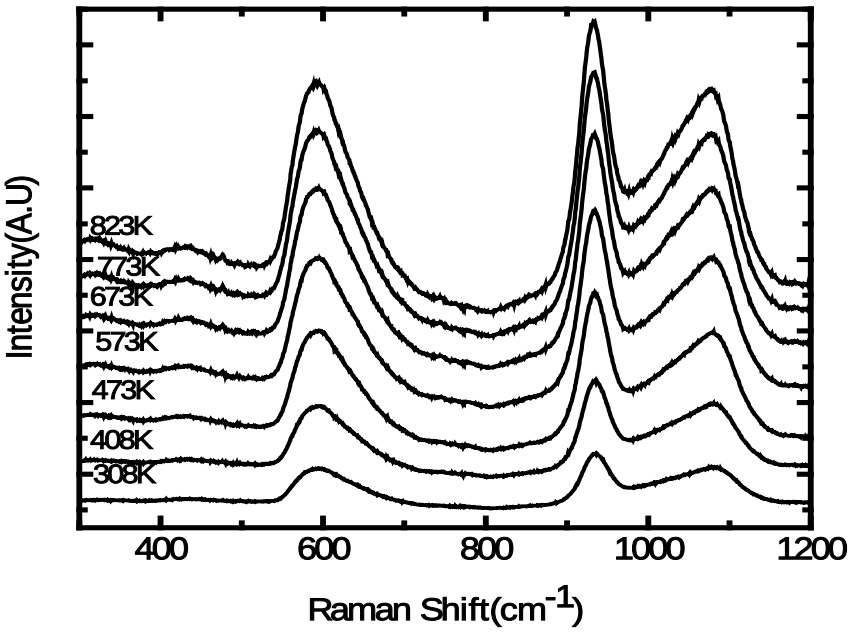

Figure 3.7: *Temperature-dependent Raman Spectra for 55S4.3 normal glass sample.*

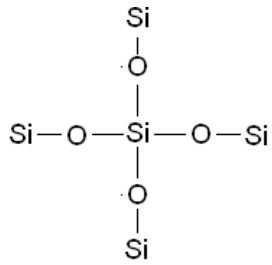

Q^4 NBO/Si=0

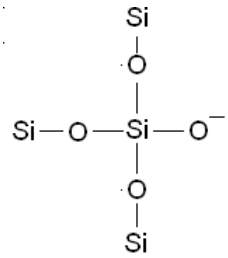

Q^3 NBO/Si=1

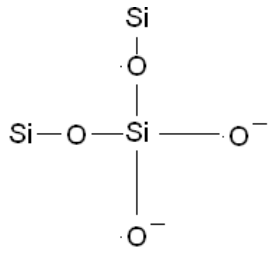

Q^2 NBO/Si=2

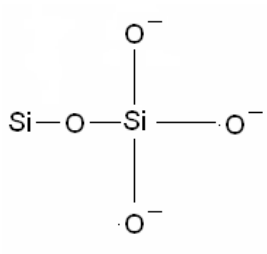

Q^1 NBO/Si=3

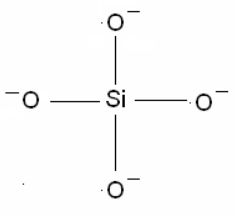

Q^0 NBO/Si=4

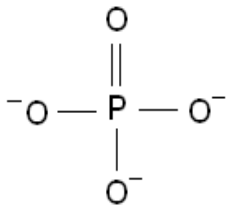

ORTHOPHOSPHATE (Q_P^0)

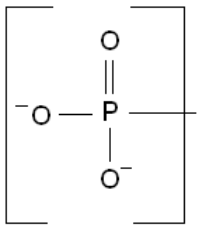

PYROPHOSPHATE (Q_P^1)

Figure 3.8: *Various phosphate and silicate Q^n species species present in glass system under investigation.*

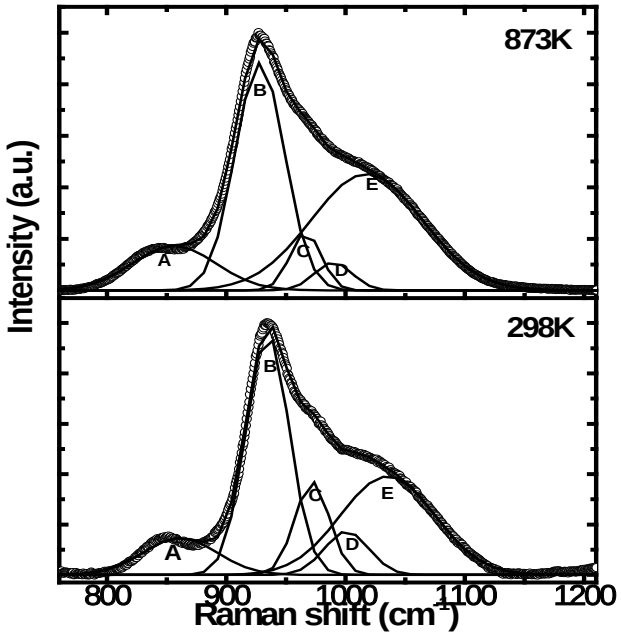

Figure 3.9: *Deconvoluted Raman spectra of 45S5 glass sample measured at 298K and 873K (open symbols) and a representative fitting (lines) with five Gaussian bands to resolve the fine structure.*

In order to obtain more detailed information about the Q^n distribution, the frequency range of 750 to 1200 cm^{-1} was fitted to five or six Guassian lines. A representative example of deconvolution procedure for 45S5 glass at two different temperatures (298 and 873K) is illustrated in the Figure 3.9.

The individual band assignments and the fitting parameters (peak position, width, and area) of the Raman data are summarized in Table 3.1.

Table 3.1: *Q^n distribution of 45S5 Normal glass sample at 298K and 573K Obtained by Deconvolution procedure*

Peak assignment	Peak identity	298K			873K		
		Raman shift $(cm)^{-1}$	FWHM $(cm)^{-1}$	Normalized peak area	Raman shift $(cm)^{-1}$	FWHM $(cm)^{-1}$	Normalized peak area
A	Q^0	850	62.09	11.34	850	69.88	15.08
B	Q^2	945	36.07	43.22	945	41.61	46.05
C	Q_P^0	970	29.04	13.46	970	26.09	7.33
D	Q_P^1	1000	37.39	8.10	1000	31.52	4.30
E	Q^3	1080	78.76	38.68	1080	93.09	52.72

We show the temperature dependence of relative abundance of different Q^n species in all three normal glass compositions obtained by *in situ* high temperature Raman spectroscopy in Figure 3.10. The calculated relative abundance of different Q^n species at room temperature is corroborate with those reported earlier by experimental and MD simulation results [26-28]. Remarkably, it is interesting to note that the temperature variation of anionic species (Q^3 and Q_P^0) is more significant in 45S5 glass than 55S4.3 and 60S3.8 glass samples.

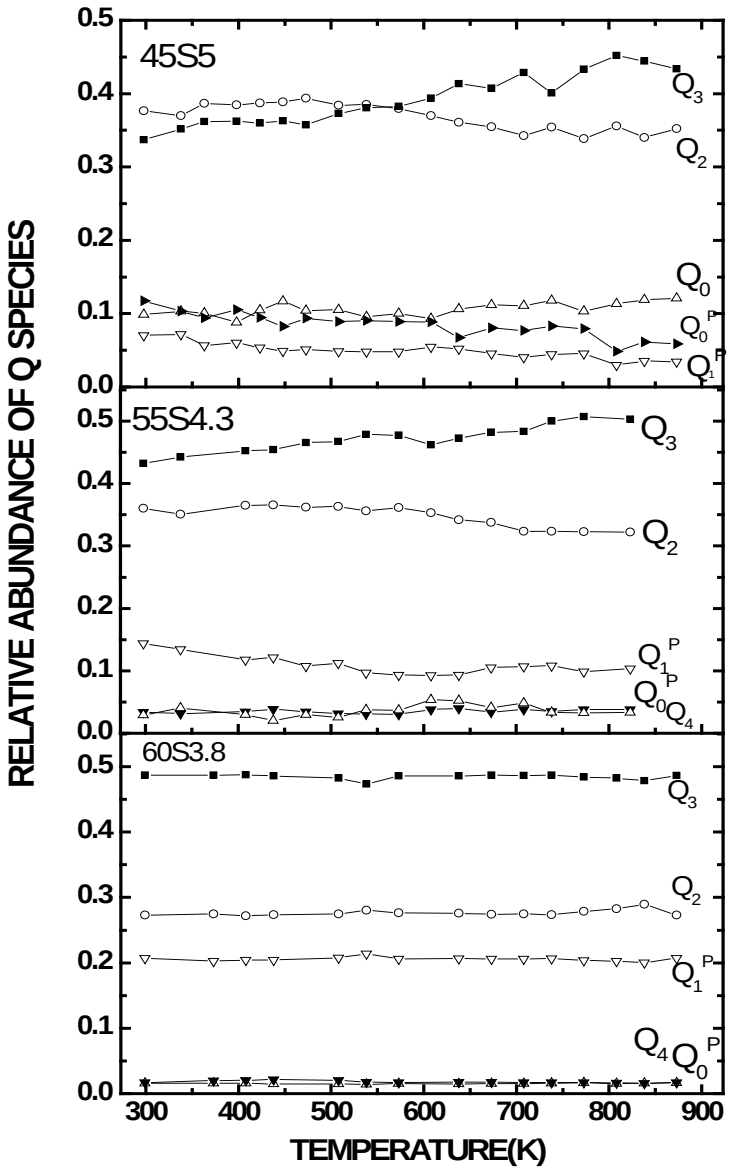

Figure 3.10: *Distribution of various structural units (Q^n) and their relative abundance as a function of temperature in 45S5, 55S4.3 and 60S3.8 normal glass samples.*

Thus, the temperature dependence of equilibrium reaction between the anionic species is given by

$$Q_P^O + Q^4 \longleftrightarrow Q_P^1 + Q^3 \quad (3)$$

and with an increase of temperature the equilibrium reaction shifts to right-hand side. It is evident that the temperature variation of the Q^n species is strongly associated with the observed nAB in the dc conductivity. It follows from the Eqn. 3 that as the phosphate species undergo the polymerization and the silicate network becomes depolymerised with an exchange of oxygen between them. Additionally, it is interesting to note that these findings have been corroborated by the earlier reports on alkali silicate glasses with small amount of P_2O_5 [24, 25]. The dynamical changes in the P-Si connectivity are possible due to the higher flexibility of the silicate network structure [29, 30]. On the other hand, in potassium silicate glasses the observed nAB shows the negative curvature with increasing temperature [17] and the temperature dependence of equilibrium reaction follows

$$2Q^3 \longleftrightarrow Q^4 + Q^2 \quad (4)$$

and the reaction shifts to right-hand side with an increase of temperature [31]. Thus, we state that the deviation from Arrhenius behaviour (both positive and negative curvatures) is directly related to the local structural changes with an increase of temperature. In the present investigation with increasing temperature, $Si_2O_5^{2-}$ Q^3 units are increased and the process is reversible; in binary potassium silicate glasses with an increase of temperature SiO_3^{2-}(Q^2) units are formed at the expanse of Q^3 units and the process is irreversible. It is important to note that the structural conversion, i.e., species exchange, discussed above should be considered separate from the structural relaxation which gives rise to the glass transition phenomenon. In this context, we have tested the effect of annealing on local structure with the observed nAB by carrying out high temperature Raman studies on annealed samples as well. In Figure 3.11 we present the temperature dependence of relative abundance of Q^n species in 45S5 and 55S4.3 annealed glass samples.

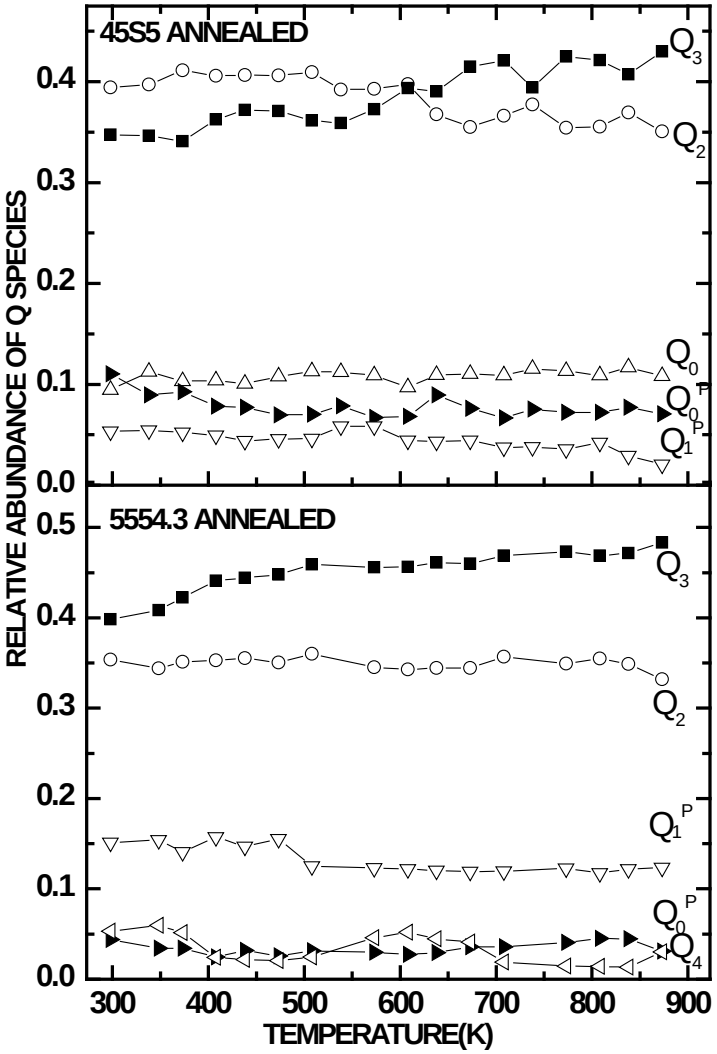

Figure 3.11: *Distribution of various structural units (Q^n) and their relative abundance as a function of temperature in 45S5 and 55S4.3 annealed glass samples.*

We find that the temperature dependence of Q^n species variations in annealed glass sample is indistinguishable from those observed in normal glass samples. Therefore, we analyze, in the following, the influence of the glass structure on the dynamics of the mobile ions with respect to the observed nAB. The detailed structure and dynamics of 45S5 glass and melts have been explored by *ab initio* MD simulation techniques [28, 29]. These studies suggest that in the melt there is significant amount of structural or coordinative defects exists and decreases upon cooling. The creation or removal of these defects occurs through Si-O bond formation or dissociation, reflects the frequent exchange between the different species, which in turn dynamically modify the intertetrahedral connectivity of silicate groups. The

equilibrium reaction given in Eqn.3 directly implies that the increase of temperature leads to the increased concentration of Q^3 species at the expense of Q^4. In addition to this equilibrium reaction (Eqn.3), we suggest that there could be an additional species exchange between adjacent silicate units itself via transfer of oxygen anions between them, which we are unable to detect from the present study.

In the dc conductivity regime, we probe the long-range ion transport rather local hopping of ions and the energy barriers involved in this case could be highest barrier between the two sites (i.e., ion hops are successful). In a disordered potential landscape with site energy disorder where the ions move in, the energy barrier associated with Q^3 species would be larger than Q^2 species, since in the later case would involve local hops. Based on the above results, a glass which show the negative slope in the Arrhenius plot is due to decrease in the concentration of vacant site for ion hopping with high energy barrier or increased concentration of local hoping sites with less energy barrier (Q^2). On the other hand, the positive slope in Arrhenius plot is due to an increased concentration of Q^3 species with temperature causing increased concentration of more vacant sites for ion hopping with highest energy barrier; there are even higher barrier but these are unrelated because the ion has to move round them.

The available number of sites and its variation with temperature strongly depends on the distribution of site energy of the disordered potential landscape. In the framework of the 'vacancy-like' transport concept, this implies a temperature-independent number of empty sites at low temperatures and increased number of empty sites (Q^3) at higher temperatures. Recently, several theoretical groups have used MD simulation as tool to investigate ion transport mechanisms in glasses and have found that only few empty sites for the ions exist [32-35]. This bears an analogy to the existence of a small number of vacancies in crystalline materials. Therefore, a 'vacancy-like transport mechanism' in glass has been postulated. Additionally, the concept of 'vacancy-like transport mechanism' has been used to explain nAB in FIC glasses by analyzing the frequency dependent conductivity data using scaling procedure [36]. In the present study, we find that creation of additional sites at high temperatures is due to the species exchange between silicate and phosphate anionic

units. Thus, it seems plausible that this type of structural conversion leads to more empty ionic sites with high energy barrier in the glass network at high temperatures and leads to nAB in the dc conductivity.

3.4 CONCLUSIONS

In summary, we have shown that the dc conductivity of alkali ion conducting silicate glasses found to exhibit nAB with a positive curvature in the Arrhenius plot. The observed nAB is completely reversible and aided by the exchange of structural species between silicate and phosphate anionic groups. Based on the available structural data, we provide an explanation for nAB with positive and negative curvatures observed in different ion conducting glasses. The present results directly support the 'vacancy-like' transport mechanism postulated by different theoretical studies on ion conducting glasses. We believe that these new correlations will bring more insights and understanding for the optimization of amorphous ionic conductors. For drawing a more quantitative comparison between the exchange of various other structural species and ion transport, local probes such as in situ high temperature NMR studies would be highly desirable.

REFERENCES

[1] C.A.Angell, C. Liu, E. Sanchez, Nature (London) 362(1993)137-139.

[2] A.M.Christie, S.J. Lilley, E. Staunton, Y.G. Andreev, P.G.Bruce, Nature (London) 433(2005)50-53.

[3] J. Horbach, W. Kob, K. Binder, Phys. Rev. Lett. 88(2002)125502.

[4] P. Jund, W. Kob, R. Jullien, Phys. Rev. B 64(2001)134303.

[5] M.E. Brandriss, J.F. Stebbins, Geochem. Cosmochim. Acta 52(1998)2659-2670.

[6] E.V. Dubinsky, F.F. Stebbins, Amer. Mineral. 91(2006)753-761.

[7] J.F. Stebbins, S.E. Ellsworth, J. Am. Ceram. Soc. 79(1996)2247-2256.

[8] P.K. Gupta, M.L. Lui, P.J. Bray, J. Am. Ceram. Soc. 68(1985)C-82.

[9] S. Sen, Z. Xu, J.F. Stebbins, J. Non-Cryst. Solids 226(1998)29-40.

[10] D. Chen, H. Miyoshi, H. Masui, H. Akai, T. Yazawa, J. Non-Cryst. Solids 345 & 346(2004)104-107.

[11] M.D. Ingram, C. Vincent, A. Wandless, J. Non-Cryst. Solids 53(1982)73-82.

[12] J. Kincs, S.W. Martin, Phys. Rev. Lett. 76(1996)70-73.

[13] C. Leon, J. Santamaria, M.A. Paris, M. A. J. Sanz, J. Ibarra, A. Varez, J. Non Cryst. Solids 235-237(1998)753-760.

[14] K.L. Ngai, A.K. Rizos, Phys. Rev. Lett. 76(1996)1296.

[15] P. Maass, M. Meyer, A. Bunde, W. Dieterich, Phys. Rev. Lett. 77(1996)1728.

[16] S.W. Martin, J. Schrooten, B. Meyer, J. Non-Cryst. Solids 307-310(2002) 981-991.

[17] M. Malki, M. Micoulaut, F. Chaimbault, Y. Vaills, Phys. Rev. Lett. 96(2006)145504-145507.

[18] S. Murugavel, B. Roling, Phys. Rev. B 76(2007) 180202(R).

[19] A. Obata, S. Nakamura, K. Yamashita , Biomaterials 25 (2004)5163-5179.

[20] C.R. Mariappan, D.M. Yunos, A.R. Boccaccini, B. Roling, Acta Biomater. 5(2009) 1274-1283.

[21] F.V. Natrup, H. Bracht, S. Murugavel, B. Roling, Phys. Chem. Chem. Phys. 7(2005)2279-2286.

[22] E.M. Tanguep Njiokep, A.W. Imre, H. Mehrer, J. Non-Cryst. Solids 354(2008) 355-359.

[23] S.A. Brawer, W.B. White, J. Chem. Phys. 63(1975)2421-2432.

[24] B. Mysen, Amer. Mineral. 81(1996)1531-1534.

[25] H. Grussaute, L. Montagne, G. Palavit, J.L. Bernard, J. Non-Cryst. Solids 263&264(2000)312-317.

[26] L. Linati, G. Lusvardi, G. Malavasi, L. Menabue, M.C. Menziani, P. Mustarelli, A. Pedone, U. Segre J. Non-Cryst. Solids 354(2008)84-89.

[27] A. Angelopoulou, V. Montouillout, D. Massiot, G. Kordas, J. Non-Cryst. Solids 354(2008)333-340.

[28] A. Tilocca, A.N. Cormack, N.H. de Leeuw, Chem. Mater. 19(2007)95-103.

[29] A. Tilocca, Phys. Rev. B76 (2007)224202(R).

[30] D. Miyabe, M. Takahashi, Y. Tokuda, T. Yoko, T. Uchino, Phys. Rev. B 71(2005)172202(R).

[31] T. Maehara, T. Yano, S. Shibata, M. Yamane, Philos. Mag. 84(2004) 3085-3099.

[32] A.N. Cormack, J. Du, T.R. Zeitler, Phys. Chem. Chem. Phys. 4(2002)3193-3197.

[33] H. Lammert, M. Kunow , A. Heuer, Phys. Rev. Lett. 90(2002)215901(R).

[34] H. Lammert, A. Heuer, Phys. Rev. Lett. 90(2010)125901.

[35] J.C. Dyre, J. Non-Cryst. Solids 324(2003)192-195.

[36] S. Murugavel, Phys. Rev. B 72 (2005) 134204(R).